



Glacial deep ocean deoxygenation driven by biologically mediated air-sea disequilibrium

Ellen Cliff^{1™}, Samar Khatiwala¹ and Andreas Schmittner¹

Deep ocean deoxygenation inferred from proxies has been used to support the hypothesis that a lower atmospheric carbon dioxide during glacial times was due to an increase in the strength of the ocean's biological pump. This relies on the assumption that surface ocean oxygen (O_2) is equilibrated with the atmosphere such that any O_2 deficiency observed in deep waters is a result of organic matter respiration, which consumes O_2 and produces dissolved inorganic carbon. However, this assumption has been shown to be imperfect because of disequilibrium. Here we used an Earth system model tuned to a suite of observations, which reproduces the pattern of glacial-to-Holocene oxygenation change seen in proxy data, to show that disequilibrium plays an important role in glacial deep ocean deoxygenation. Using a novel decomposition method to track O_2 , we found a whole-ocean loss of 33 Pmol O_2 from the preindustrial to the Last Glacial Maximum despite a 27 Pmol gain from the increased solubility due to cooler temperatures. This loss was driven by a biologically mediated O_2 disequilibrium, which contributed 10% of the reduction of the O_2 inventory from the solubility equilibrium in the preindustrial compared with 27% during the Last Glacial Maximum. Sea ice and iron fertilization were found to be the largest contributors to the Last Glacial Maximum deoxygenation, which occurs despite overall reduced production and respiration of organic matter in the glacial ocean. Our results challenge the notion that deep ocean glacial deoxygenation was caused by a stronger biological pump or more sluggish circulation, and instead highlight the importance and previously underappreciated role of O_2 disequilibrium.

xygen (O_2) is fundamental for life in the ocean, and is intrinsically connected with the cycling of carbon through photosynthesis: carbon dioxide (CO_2) is fixed and O_2 produced by phytoplankton in the surface ocean, and O_2 is consumed and dissolved inorganic carbon (DIC) released when organic matter is broken down by microbial respiration throughout the ocean. This transfer of carbon to the deep ocean is termed the 'soft-tissue pump': O_2 can thus be a powerful tool to understand the cycling and storage of respired carbon in the ocean, the quantification of which is important to answer fundamental questions of carbon cycling under different climate states.

The Last Glacial Maximum (LGM; ~20,000 years BP) is the most recent example of a relatively stable, different climate state. This period saw global mean ocean temperatures 2.5°C colder than those in preindustrial times, and atmospheric CO₂ 90 ppm lower^{1,2}. Deep ocean deoxygenation relative to the preindustrial has been observed globally using a variety of O₂ proxies from seafloor sediments^{3,4}. These results are used to support the hypothesis that deep ocean carbon storage in the LGM was the result of a stronger or more efficient soft-tissue carbon pump^{3,5-9}, which could partially explain the reduction of atmospheric CO₂ during glacial periods^{1,2}. It was recently demonstrated¹⁰ with an observationally constrained model that glacial carbon storage in the deep ocean was enhanced by air-sea disequilibrium of CO2 caused by temperature changes and iron fertilization, whereas changes in circulation and sea ice extent, previously regarded as the primary drivers, played a minor role. Importantly, atmospheric CO₂ was reduced through increased deep ocean carbon storage, even as export production in the modelled glacial ocean decreased. However, deep ocean O2 still decreased in the model. Here we show that the air-sea disequilibrium of O₂ can be a substantial part of the oxygen budget, and potentially decouple oxygen from

biological carbon storage and confound efforts to use it as a proxy to reconstruct past variations in the efficiency of the biological carbon pump.

Owing to the more rapid air-sea gas equilibration timescale of O₂ relative to CO₂ (a few weeks versus about a year¹¹), O₂ disequilibrium is often considered a minor component of the O₂ budget^{6,12,13}. In the modern ocean, observations show summertime O₂ oversaturation caused by photosynthesis, whereas wintertime undersaturation at high latitudes is driven by heat fluxes, extensive sea ice cover and wind-driven upwelling of oxygen-depleted deep waters^{14,15} (Fig. 1). The deep ocean is supplied with O₂ through subduction at high latitudes in the wintertime, when cold, dense water masses develop after deep convection and sea ice formation. The effect of disequilibrium may be greater in the Southern Ocean, where oxygen-depleted intermediate and deep waters upwelling to the surface have a shorter surface exposure time than those in the North Atlantic¹³. The propagation of undersaturated waters from the Southern Ocean into the interior, a phenomenon supported by observations¹⁶, could have an especially large impact on the ocean's O₂ inventory because a large fraction of the deep ocean is ventilated from the Southern Ocean¹⁷. The ocean model used in this study shows reasonable agreement with the observed surface O₂ saturation (Fig. 1). Although the modelled wintertime disequilibrium in the northern North Atlantic is larger than that observed, which probably leads to an overestimated disequilibrium in North Atlantic Deep Water, in the high latitude wintertime Southern Ocean, an important region of deep and bottom water formation, the (few) Southern Ocean wintertime measurements available show a greater undersaturation than that of the model.

The Southern Ocean is known to be important in glacial CO₂ storage^{2,7} and the mechanisms that affect LGM carbon disequilibrium

¹Department of Earth Sciences, University of Oxford, Oxford, UK. ²College of Earth, Ocean, and Atmospheric Sciences, Oregon State University, Corvallis, OR, USA. [™]e-mail: ellen.cliff@earth.ox.ac.uk

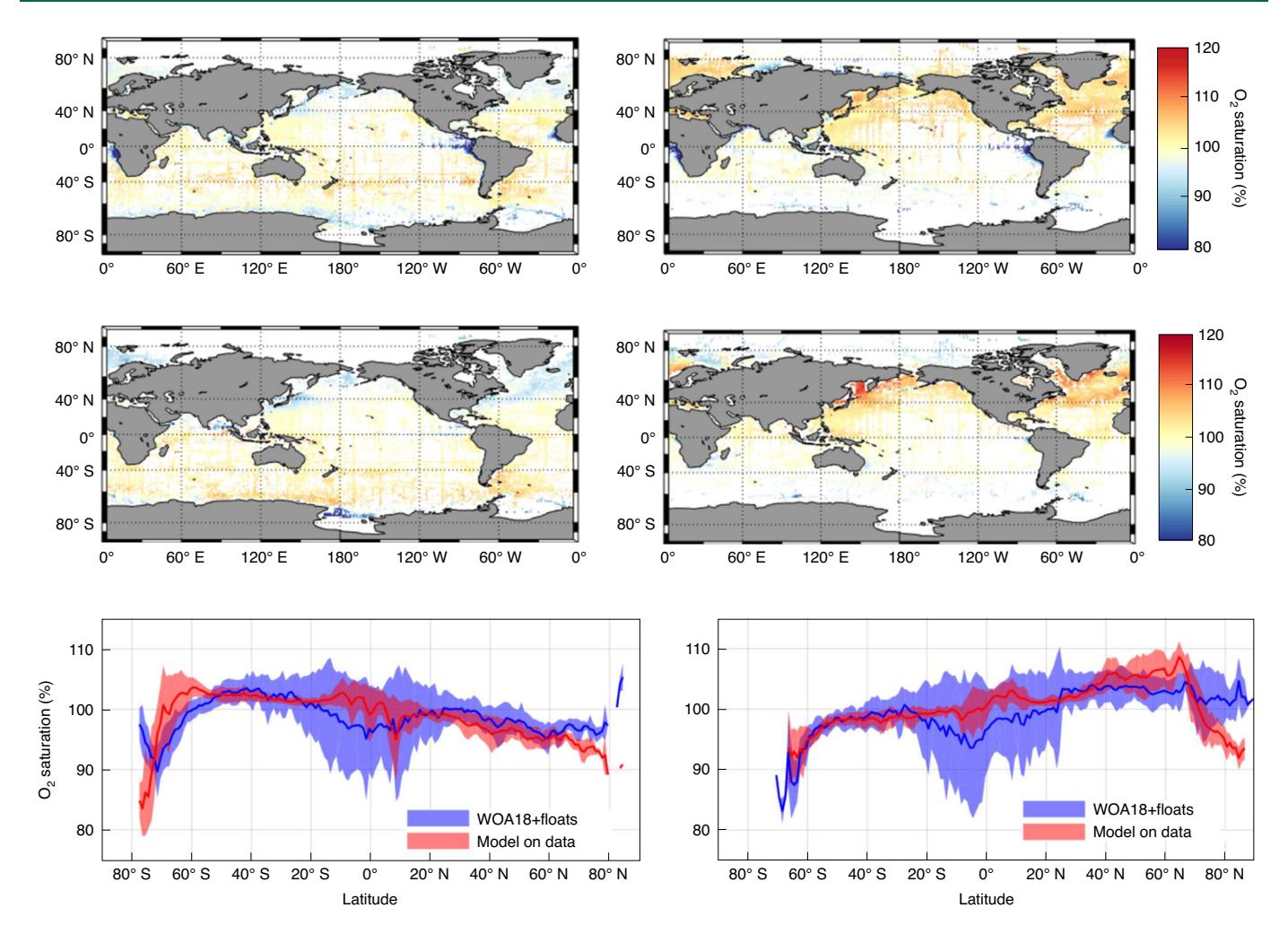


Fig. 1 Comparison of surface O₂ saturation from a compilation of the World Ocean Atlas 2018 (WOA18 (ref. ⁴⁸))+float data (University of Washington Argo O₂ reanalysis ⁴⁹, and quality-controlled data from the SOCCOM (Southern Ocean Carbon and Climate Observations and Modeling) programme ⁵⁰). World Ocean Atlas 2018+float surface O₂ saturation data (%) were spatially binned into 1×1° WOA grid boxes, and a seasonal climatology was made by binning data temporally by month (top row). Grid boxes without any measurements were discarded. Results shown here are for the Northern Hemisphere winter and Southern Hemisphere summer (December-January-February (DJF)) (left column), and the Northern Hemisphere summer and Southern Hemisphere winter (June-July-August (JJA)) (right column). Surface O₂ saturation values are shown for observations (top row) and the model's PIC simulation interpolated to the locations where observations are available (middle row). The bottom row shows a comparison of zonal mean surface O₂ saturation in the observations and model at the location of observations, with one standard deviation of the zonal data shaded. Note that observations for the Southern Ocean are sparse, particularly in the winter months, as are those in the Arctic, where large model-data differences are seen and may be influenced by sampling biases in conditions without or with thin sea ice because research vessels are limited in accessing regions with thick sea ice cover.

were recently modelled10. A number of studies showed that O2 disequilibrium can be non-negligible^{14,18}, but a mechanistic study of LGM deoxygenation is lacking. Although some studies assumed that O2 disequilibrium does not vary greatly between the modern and LGM climate states^{6,13}, others suggested that, like carbon, O_2 disequilibrium could be larger in the $\widetilde{\mathrm{LGM}}^{8,19}.$ Here we apply a comprehensive method for decomposing O2 to quantify the magnitude of O2 disequilibrium and investigate the processes that drive glacial deoxygenation. This approach allows the effect of air-sea disequilibrium to be tracked through model simulations, and for physical and biological effects to be separated. The method was applied to biogeochemical fields simulated by two different configurations of the UVic Earth System Model²⁰ coupled to the Model of Biogeochemistry and Isotopes²¹. The configurations, that represent preindustrial control (PIC) and LGM conditions, were tuned to a suite of modern biogeochemical and LGM sedimentary isotope records22 (Methods).

Oxygen decomposition analysis

To accurately track the cycling of O_2 in the model (Fig. 2 and Methods) we express the concentration of O_2 as:

$$O_2 = O_{2,eq} + O_{2,dis,phy} + O_{2,dis,bio} + O_{2,soft}$$
 (1)

Here, $O_{2,eq}$ is the theoretical O_2 concentration of the water parcel in solubility equilibrium with the atmosphere, $O_{2,dis,phy}$ and $O_{2,dis,bio}$ are the physical and biological components, respectively, of disequilibrium ($O_{2,dis}$) that lead to the deviation of surface O_2 from $O_{2,eq}$. $O_{2,soft}$ is the O_2 consumed when organic matter is broken down and accumulates as a deficit in the ocean interior while regenerated DIC, nitrate and phosphate accumulate. Unlike nutrients, O_2 and CO_2 can exchange with the atmosphere at the surface, which affects the preformed O_2 and DIC pools.

Disequilibrium at the surface is driven by both sea surface temperature gradients and upwelling of waters depleted in O_2 due to

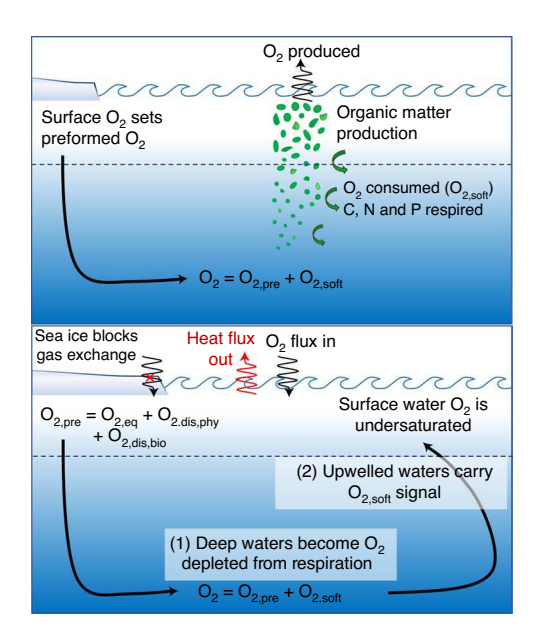


Fig. 2 | Schematic of the O2 decomposition used in this study. The top panel shows the standard decomposition (Methods) of O_2 into preformed O_2 ($O_{2,pre}$), set at the surface and subsequently transported conservatively into the interior by the circulation, and $O_{2,soft}$: O_2 consumed during the respiration of organic matter (which is therefore negative)^{14,18}. The sum of these terms gives the total O_2 . The bottom panel shows the extended decomposition that incorporates surface disequilibrium, which causes deviation from the equilibrium preformed concentration ($O_{2,eq}$). $O_{2,dis,phy}$ is caused by surface heat fluxes. Biological processes can also cause disequilibria ($O_{2,dis,bio}$) by photosynthesis at the surface, which creates a positive disequilibrium, or as a result of the upwelling of waters depleted in O_2 due to respiration, which leads to a negative disequilibrium. Waters upwelling in the Southern Ocean have a short surface exposure time so can have substantial $O_{2,dis,bio'}$ which may be enhanced by sea ice, which blocks gas exchange.

biological consumption 14,19 . To distinguish between these mechanisms, we carried out a parallel set of simulations in which biogeochemical processes were switched off. The difference between the full physical–biogeochemical and the physics-only simulations allowed us to separate the $O_{2,\rm dis,bio}$ and $O_{2,\rm dis,phy}$ contributions to $O_{2,\rm dis}$. Physical disequilibrium occurs when waters moving poleward do not equilibrate fully as they lose heat, whereas biologically mediated disequilibrium occurs when waters depleted in O_2 from either $O_{2,\rm soft}$ or $O_{2,\rm dis,bio}$ are entrained or upwelled to the surface. Once at the surface, the part of this deficit that is not replenished through air–sea gas exchange is relabelled as $O_{2,\rm dis,bio}$ and becomes part of the preformed O_2 pool that is resubducted into the interior.

We note that $O_{2,soft}$ is negative, as generally are $O_{2,dis,phy}$ and $O_{2,dis,bio}$, that is, they reduce the O_2 inventory of the ocean from $O_{2,eq}$. A similar approach was previously applied to carbon using the same model O_2 , which allows for the comparison of O_2 and carbon.

Oxygen distribution in the preindustrial and LGM

The O_2 inventory and its components for the PIC and LGM are shown in Table 1 and in Fig. 3. In the preindustrial configuration, the total ocean O_2 content is 266 Pmol O_2 (global mean concentration of 196 mmol m⁻³), similar to estimates of the modern ocean inventory (227 Pmol O_2) (ref. ²³) and within the range of CMIP5 models (136–231 mmol m⁻³) (ref. ²⁴). As expected, $O_{2,eq}$ is the largest component; all the other components reduce the inventory so that the total O_2 is 40% of the equilibrium value. Two-thirds of the reduction is due to consumption during respiration ($O_{2,sof}$), with

Table 1 | O₂ decomposition for the PIC and LGM simulations

	O ₂	$O_{2,eq}$	$O_{2,dis,phy}$	O _{2,dis,bio}	O _{2,soft}
PIC (Pmol)	266	458	-12	-49	-127
PIC (mmol m ⁻³)	196	337	-9	-36	-94
LGM (Pmol)	233	482	-9	-132	-104
LGM (mmol m ⁻³)	172	355	-7	-97	-77
LGM - PIC (Pmol)	-33	+24	+3	-83	+23
LGM - PIC (mmol m ⁻³)	-24	+18	+2	-61	+17

Results are shown in terms of the total inventory (Pmol) and global mean concentration (mmol m^{-3}). Negative values indicate the deficit of O_2 that result from incomplete equilibration or consumption during respiration. The differences between the LGM and PIC inventory values are also shown; positive (negative) values indicate more (less) O_2 in the LGM than in the PIC.

the remaining decrease due to disequilibrium, of which 80% is biologically mediated. The spatial distribution and magnitude of O_{2,dis} (Supplementary Fig. 2) are similar to those in a previous study¹⁴.

The glacial ocean has ~12% less O_2 (Fig. 3), consistent with proxy-based reconstructions that show widespread deep ocean deoxygenation^{3,4,6,8,25–32}. The majority of the proxy data are qualitative, which indicates whether O_2 was higher or lower in the LGM (20–22 kyr BP) relative to the Holocene (5–10 kyr BP). The model captures the general pattern of upper ocean oxygenation and deep ocean deoxygenation in the LGM relative to the PIC, although it may underestimate the full magnitude of deep ocean deoxygenation (Supplementary Information).

LGM O₂ decreases despite the cooler temperatures that enhance O_2 solubility and thus $O_{2,eq}$ (by ~5%) (Fig. 3 and Supplementary Fig. 6). O2 is also enhanced by increases in O2,dis,phy and O2,soft both of which are less negative in the LGM (by ~25% and ~20%, respectively). Globally, export production in the LGM simulation is reduced, which causes this O_{2,soft} increase. Although there is no corresponding observational estimate, regional observations do exist33 and the model captures these variations reasonably well (Supplementary Fig. 3). The only component of the O₂ budget that drives glacial deoxygenation is O_{2.dis,bio}, which nearly triples in the glacial ocean (to -132 Pmol), overwhelming increases brought about by changes due to physical processes and organic matter export. The decomposition of O2 into physical and biological components enables a more complete appreciation for the glacialinterglacial difference in O2 distributions that has not been demonstrated before. That the decline in O₂ during the LGM is driven by biologically mediated disequilibrium is a novel finding.

Drivers of LGM deoxygenation

To understand the mechanisms behind glacial deoxygenation, a series of perturbation experiments was performed in which a single parameter (temperature, circulation, sea ice or iron fertilization) in the preindustrial configuration was changed to its LGM condition and the model run to steady state. An additional 'All' experiment was carried out in which these parameters (and salinity) were simultaneously changed. Figure 4 shows the change in the inventories of the $\rm O_2$ components due to these perturbations. To probe the dependence of the response on the base state of the model¹⁹, a 'reverse' set of experiments was also run in which PIC fields were used to perturb the LGM state (Supplementary Figs. 11–23).

In the LGM temperature perturbation experiment, a non-uniform temperature change consistent with reconstructions 34,35 was imposed, which increased the ocean's $\rm O_2$ inventory by 30 Pmol. The principal effect was an increase in $\rm O_{2,eq}$ (by 31 Pmol) through enhanced solubility. Changes in $\rm O_{2,eq}$ closely followed the pattern of temperature change with the largest differences seen in the North Atlantic (Supplementary Fig. 24). Weakened meridional sea surface temperature gradients and

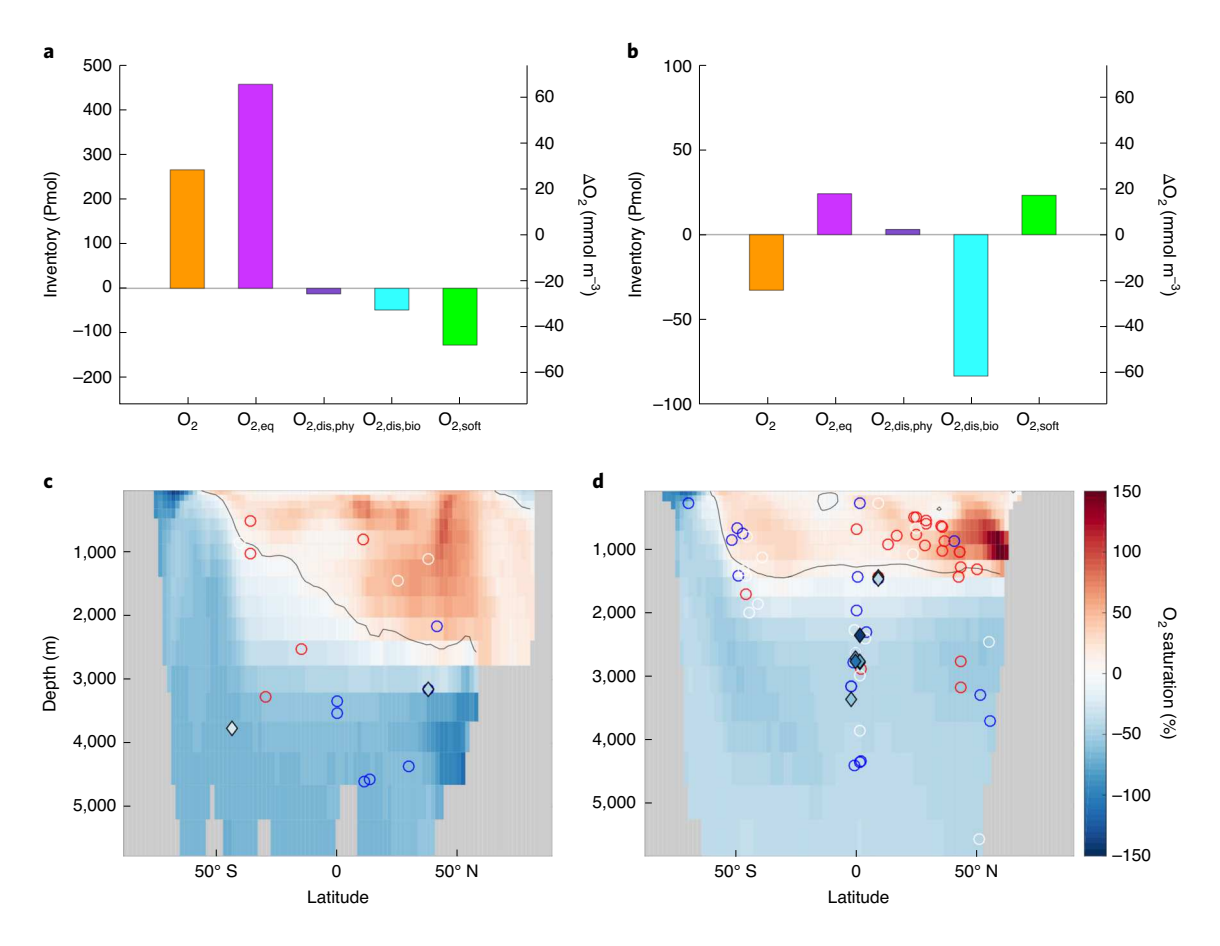


Fig. 3 | The components of O₂ in the PIC and LGM relative to PIC. a,b, Oxygen decomposition for the PIC equilibrium simulation (**a**) and the difference between the LGM and PIC equilibrium simulations (**b**) are shown as inventory values. The equivalent deep ocean inventory decomposition plots are in Supplementary Fig. 5. **c,d**, Zonal mean sections of the LGM – PIC Δ O₂ are shown for the Atlantic (**c**) and Pacific (**d**) oceans. Proxy-based reconstructions of Δ O₂ from the LGM to the Holocene are included. Blue (red) circles indicate a qualitative decrease (increase) in O₂ from the Holocene to the LGM_{3.6,8,25,26,28,29,31}. Diamonds represent a quantitative O₂ change (mmol m⁻³) (refs. ^{4,27,29,30}) using results of the infaunal–epifaunal foraminifera δ¹³C method that are within the range of a previously published calibration²⁷ and are shaded according to the colour scale. The quantitative data point shown in the southern Atlantic was calculated using the modern O₂ concentration at the core site as data were not available for the Holocene²⁵ and recalculated as in Gottschalk et al.⁵¹. See the Supplementary Information for further comparison of the model and reconstructions.

heat fluxes at high latitudes reduced the heat flux-driven undersaturation, which caused $O_{2,dis,phy}$ to become less negative south of ~60° S. The resulting small (8 Pmol) increase in oxygen was somewhat countered by biological factors. Cooler temperatures deepened the remineralization depth³6, which reduced O_2 consumption in the upper ocean and increased it in the deep ocean (Supplementary Fig. 10), which led to a global decrease (by 5 Pmol) in $O_{2,soft}$. A similar decomposition applied to carbon showed that temperature was a major cause of atmospheric CO_2 drawdown (by 45 ppm) due to the enhanced solubility and physical disequilibrium 10 , which illustrates that carbon and oxygen disequilibrium are controlled by different processes.

The simulated LGM ocean was characterized by a weaker and shallower Atlantic meridional overturning circulation. This reduced the upwelling of nutrient-rich deep waters in the Indo-Pacific, which caused a global reduction in export production 10,37,38 . Thus, the primary effect of circulation changes was to increase the ocean's O_2 inventory by reducing O_2 consumption, a phenomenon observed most strongly in the Pacific (Supplementary Fig. 12). A smaller $O_{2,\text{soft}}$ pool and slower overturning circulation, which allowed more time for waters upwelled in the Southern Ocean to equilibrate before subduction, also reduced $O_{2,\text{dis,bio}}$.

The LGM configuration has 50% more sea ice than that in PIC, consistent with reconstructions³⁹. Sea ice blocks both air–sea

gas exchange and the penetration of light into the surface ocean. The former enhances disequilibrium by preventing equilibration of O2-depleted waters, which results in more negative O2,dis,phy and O_{2,dis,bio}, whereas the latter reduces phytoplankton growth, and hence export production and the biological consumption of O₂. To quantitatively separate these mechanisms we carried out two additional experiments in which sea ice alternatively affected only gas exchange (SI-gasx) or biology through light limitation (SI-bio) (Supplementary Figs. 16 and 18). These show that air-sea gas exchange has a much larger effect, as it reduced O2 by 81 Pmol $(\Delta O_{2,dis,phy} = -25 \text{ Pmol and } \Delta O_{2,dis,bio} = -56 \text{ Pmol})$. Light limitation has a smaller and compensating effect, as it increased O₂ by 30 Pmol $(\Delta O_{2,soft} = +15 \text{ Pmol}, \Delta O_{2,dis,bio} = +15 \text{ Pmol})$. Their net effect is additive and decreased the O2 inventory by 49 Pmol in the sea ice experiment. These changes were largely driven by greater sea ice extent in the Southern Ocean, which decreased O₂ by over 50 mmol m⁻³ in Antarctic Bottom Water in the South Atlantic (Supplementary Fig. 14). These results are consistent with previous studies that showed the large effect of Southern Ocean sea ice on O_{2.dis} (refs. ^{14,19}), although those studies did not separate biologically mediated and physical disequilibrium. Although the implementation of the sea ice effects in our model is typical of other global models, it does not include polynyas and sea ice leads, which may reduce the strength of

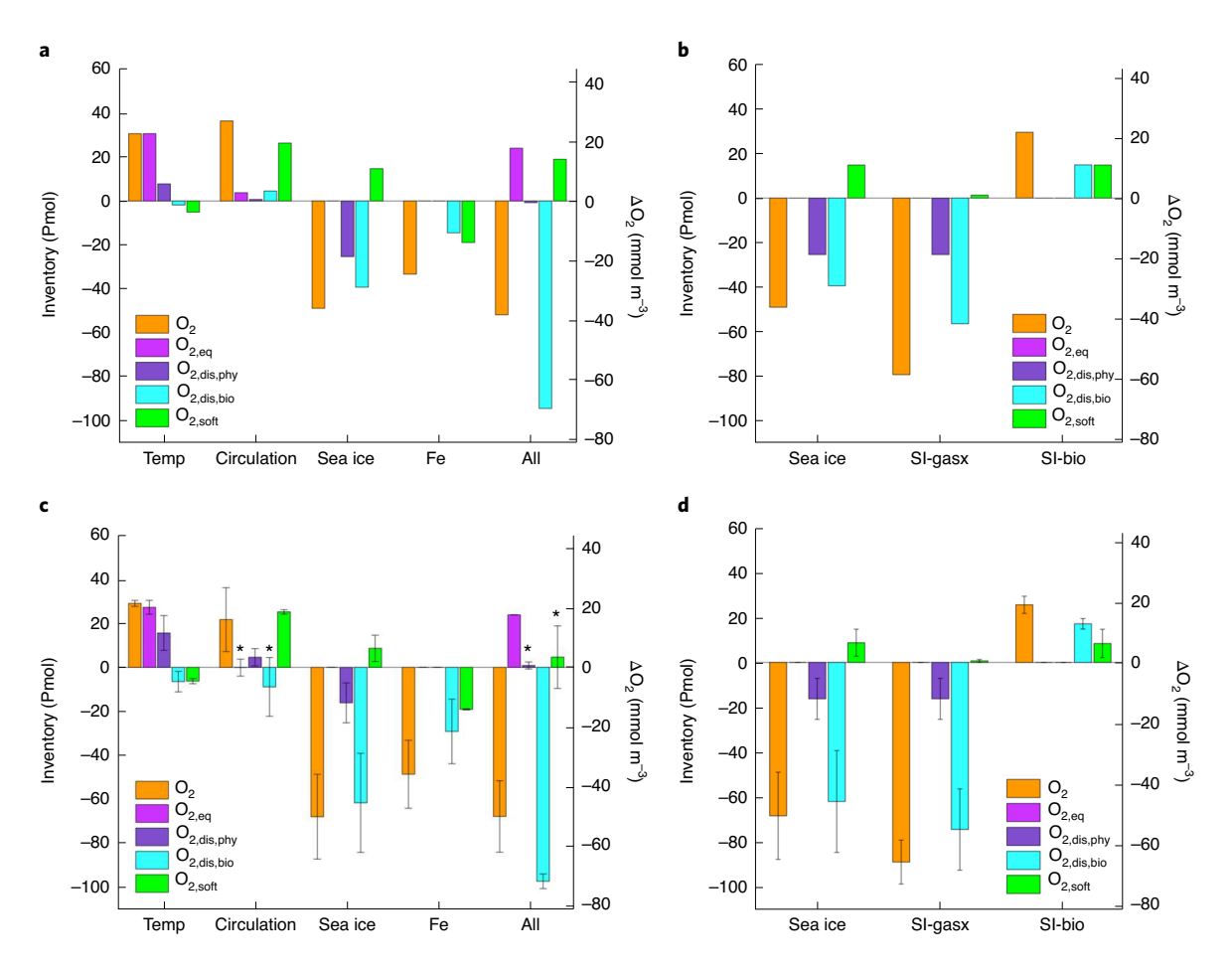


Fig. 4 | Response of PIC O_2 components to LGM perturbations and assessment of the robustness of the response of O_2 components to perturbations. **a**, Changes in the inventory following perturbation with LGM circulation, sea ice, temperature, iron, as well as 'All' perturbations (in which LGM temperature, circulation, sea ice, iron fertilization, salinity (1 PSU (practical salinity unit) increase consistent with a 110 m sea level drop) and winds were used simultaneously to perturb the PIC). Note that the 'All' experiment does not exactly reproduce the LGM equilibrium simulation as it still uses the PIC conditions for light, freshwater fluxes and subgrid bathymetry, which affect the sedimentary release of organic carbon. **b**, Changes in inventory (PIC - LGM) due to perturbations of sea ice, SI-gasx, effect of sea ice on O_2 gas exchange and SI-bio. The corresponding spatial distribution of these changes are shown in Supplementary Figs. 10–22. **c**, **d**, Assessment of robustness of the response of O_2 components to perturbations that correspond to those in **a** (**c**) and **b** (**d**) (average of PIC \rightarrow LGM and LGM \rightarrow PIC perturbations). Vertical bars are the average of the two sets of perturbation experiments (Supplementary equation (1)) and the vertical lines are the differences (Supplementary equation (2)), with the sign of the LGM to PIC perturbations reversed in both cases. The bars thus indicate whether the response is of the same or opposite sign in the two directions, whereas the lines show the average magnitude of the perturbation for the two experiment sets, such that a line that crosses the x axis implies a non-robust response to the perturbation (see Supplementary Information for details). These experiments are marked with an asterisk.

these effects as some gas exchange would still be possible and polynyas may allow for pockets of productivity. Polynyas are thought to have been present in the glacial Southern Ocean 40, although their prevalence and mechanisms of formation are not well-understood even in the modern ocean 41. Similarly, the inclusion of leads would allow for more equilibration in ice-covered waters. These processes may be an important source of uncertainty for glacial—interglacial deep ocean O_2 and carbon and their inclusion should be a priority for future modelling studies.

Consistent with evidence from Antarctic ice cores⁴² and ocean sediment records⁴³, bioavailable iron fluxes to the LGM Southern Ocean increased tenfold²². This iron fertilization enhanced export production, which depleted O_2 due to an increased consumption and biological undersaturation ($\Delta O_{2,\text{soft}} = -19 \, \text{Pmol}$; $\Delta O_{2,\text{dis,bio}} = -14 \, \text{Pmol}$; Supplementary Fig. 20). A recent study with a biogeochemical model also examined the effect of glaciogenic iron fluxes on CO_2 drawdown and deep ocean deoxygenation in the glacial ocean⁹. This showed that high Southern Ocean iron fluxes and an increase in the ocean's nutrient inventory was associated with a

third of the change in the deep ocean (below 2,000 m) apparent oxygen utilization (AOU; the deviation of O_2 from theoretical saturation) in their LGM model. Although the differences in experimental design and model base states make direct comparisons difficult, our LGM iron perturbation led to a 32 mmol m⁻³ decline in deep ocean O_2 , comparable to the 21 mmol m⁻³ change due to iron fertilization recorded by the other study (their experiment LGM_glac3%, which has the conditions most similar to ours)⁹. Our decomposition allowed us to show that almost half of the deoxygenation brought about by iron fertilization-enhanced export production was a result of biologically mediated disequilibrium, which amplified the strength of the soft-tissue pump¹³. As the other study used a similar gas exchange parameterization, it is likely to have air–sea gas disequilibrium, although the magnitude and role of disequilibrium is not known as $O_{2,pre}$ was not explicitly considered in that study.

Lastly, we consider the 'All' experiment in which the above perturbations were imposed simultaneously. The results are largely consistent with the difference between the LGM and PIC equilibrium runs (Table 1 and Fig. 3 and Supplementary Figs. 6 and 22).

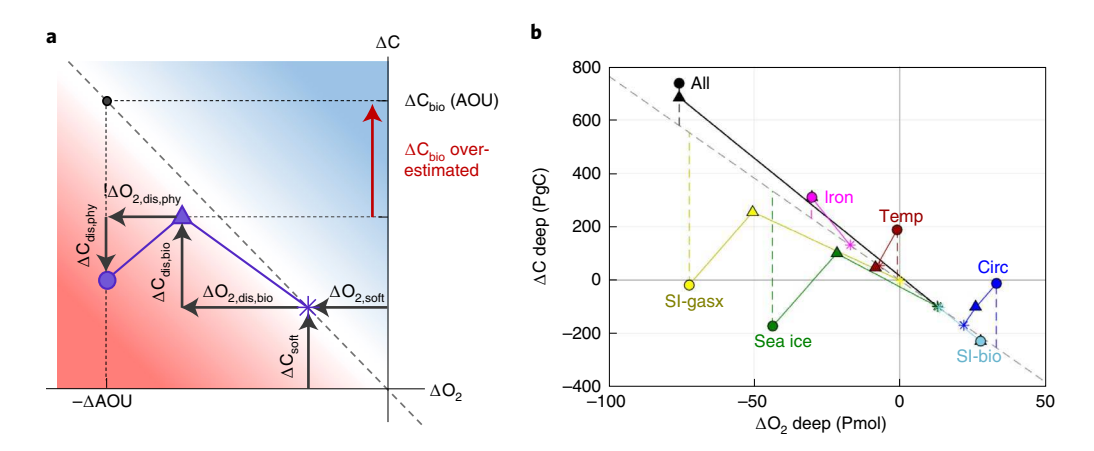


Fig. 5 | Relationship between ΔO_{2} , ΔAOU and biological carbon storage. **a**, Schematic showing how the use of AOU can lead to an over- or underestimation of biological carbon storage. For a given ΔC_{bio} (= ΔC_{soft} + $\Delta C_{dis,bio}$), the ratio of carbon to oxygen disequilibrium relative to the Redfield C:- O_2 ratio (dashed grey line) controls whether AOU under- or overestimates the change in the true biological carbon storage. In a plot of ΔAOU versus ΔC_{bio} , for points that plot in the red (blue) region below (above) the Redfield line, ΔC_{bio} (AOU) over- (under-) estimates ΔC_{bio} . Only for points that fall on the line does ΔC_{bio} (AOU) accurately quantify the biological carbon storage change. Physical disequilibrium can cause further deviation from the Redfield line, which affects ΔAOU . **b**, ΔO_2 versus ΔC in the deep ocean (below 1,000 m) for the perturbation experiments where an LGM condition is imposed on the preindustrial configuration. (For the relationship between the individual components, see Supplementary Fig. 25, and for reverse experiments with the PIC perturbations on the LGM state, see Supplementary Fig. 26). Changes are shown for the perturbations 'All' (black), sea ice (green), which is further separated into SI-gasx (yellow) and SI-bio (light blue), iron fertilization (pink), temperature (red) and circulation (dark blue). For each perturbation, three components of the carbon-oxygen system are shown: $\Delta O_{2,\text{soft}}$ and ΔC_{soft} (stars), $\Delta O_{2,\text{soft}}$ + $\Delta O_{2,\text{dis,bio}}$ and ΔC_{bio} (circles).

The dominant cause of glacial deoxygenation was a large increase in biologically mediated disequilibrium ($\Delta O_{2,dis,bio} = -94 \text{ Pmol}$). The individual perturbation experiments suggest that this was driven by Southern Ocean sea ice and iron fertilization, in line with the dipolar pattern of export production in the Southern Ocean during the LGM (Supplementary Fig. 3)10,33. Despite the increase in productivity in the Southern Ocean, global productivity was reduced in the 'All' experiment. Deoxygenation was partially compensated by an enhanced solubility because of cooling ($\Delta O_{2,eq} = +24$ Pmol) and a decrease in export production and consumption ($\Delta O_{2,soft} = +19$ Pmol) due to changes in circulation. The results of the individual perturbations did not sum to produce the 'All' experiment result because of non-linearities. For instance, in the Southern Ocean, the interplay of expanded LGM sea ice and iron fertilization may further enhance O_{2.dis,bio}, whereas weaker latitudinal temperature gradients could reduce the effect of sea ice on $O_{2,dis,phy}$

The 'reverse' set of experiments, in which the LGM state was perturbed by PIC conditions, allows us to assess the robustness of different processes in their effect on any given O_2 component. Processes that elicit a response of opposite signs in the two sets of perturbation experiments are regarded as robust, as most are found to be (Fig. 4). The exceptions are $O_{2,\text{eq}}$ and $O_{2,\text{dis,bio}}$ in the circulation experiment, and $O_{2,\text{dis,phy}}$ and $O_{2,\text{soft}}$ in the 'All' experiment. Crucially, in both sets of experiments, $O_{2,\text{dis,bio}}$ is the primary driver of O_2 changes that result from sea ice and iron fertilization, which supports our conclusion that these processes play a leading role in glacial deoxygenation.

Implications for estimates of ocean carbon storage during the IGM

The development of quantitative oxygen proxies opens up the powerful possibility of better constraining the glacial ocean carbon storage using the AOU method, the most widely used approach to estimate the inventory of respired carbon in the ocean. AOU is the difference between the saturation concentration $O_{2,sat}$ of oxygen in a water sample (estimated from its temperature and salinity) and its in situ concentration. Assuming that the water was in solubility

equilibrium when it was last at the surface of the ocean, this difference is typically attributed to oxygen consumed during soft-tissue regeneration ($C_{\rm soft}$) as the water is transported from the surface into the interior Observed higher levels of AOU in the deep ocean during the LGM relative to present day have been used to conclude that the ocean contained more $C_{\rm soft}$ during the glacial period, which led to a drawdown in atmospheric CO_2 (refs. (48,27,29)). Air–sea disequilibrium complicates this straightforward interpretation of AOU in two ways.

First, oxygen disequilibrium, shown here to be greater during the LGM, violates a key assumption of the AOU method. For instance, if surface waters are undersaturated, the true oxygen utilization will be smaller than that predicted by AOU, which leads to an overestimate of C_{soft} (refs. 10,14,18,19) (by as much as 50% in the global inventory according to a recent study10). Second, it has long been recognized that disequilibrium of CO₂ amplifies the direct effect of C_{soft} on ocean carbon storage¹³. This biologically mediated component of DIC, C_{dis,bio}, was shown to also be much larger during the LGM^{10,44}. It is therefore more appropriate to define total biological carbon storage, C_{bio}, as a sum of C_{soft} and C_{dis,bio}. Although both aspects are acknowledged as a source of uncertainty in AOU-based estimates of glacial biological carbon storage, it has been argued that, if anything, in the presence of disequilibrium AOU systematically underestimates C_{bio} (refs. ^{4,8}). Here we combine our oxygen decomposition with a previous carbon one¹⁰ to show that the extent to which proxy-based estimates of AOU capture the true glacial biological carbon storage depends sensitively on the mechanisms involved.

The change in biological carbon storage is estimated from AOU according to $\Delta C_{\text{bio}}(\text{AOU}) = R_{\text{C:}-\text{O}_2} \times \Delta \text{AOU}$, where $R_{\text{C:}-\text{O}_2}$ is a constant carbon-to-oxygen stoichiometric ratio. ΔAOU can be expressed in terms of its components as (Methods):

$$\Delta AOU \approx -\Delta O_{2,soft} - \Delta O_{2,dis,bio} - \Delta O_{2,dis,phy}$$
 (2)

which demonstrates the explicit dependence of $\Delta C_{bio}(AOU)$ on the disequilibrium components. Figure 5 shows how the cumulative

sum of the oxygen terms in equation (2) is related to that of the corresponding carbon components, ΔC_{soft} , $\Delta C_{\text{dis,bio}}$ and $\Delta C_{\text{dis,phy}}$ respectively, for the various perturbation experiments (see Supplementary Figs. 25 and 26 for the reverse experiments). By construction, ΔC_{soft} and $\Delta O_{2,\text{soft}}$, which are both diagnosed from the regenerated phosphate concentration, are exactly proportional to each other via the Redfield (stoichiometric) ratio $-R_{C:-O_2}$. When the biological disequilibrium term is added, this relationship remains strong for the 'solely' biological iron fertilization and SI-bio experiments because $\Delta C_{dis,bio}$ and $\Delta O_{2,dis,bio}$ roughly follow the Redfield line (Supplementary Fig. 25). The latter relationship becomes weaker in SI-gasx, which causes $\Delta C_{\text{soft}} + \Delta C_{\text{dis,bio}}$ to deviate from the Redfied relationship with $\Delta O_{2,soft} + \Delta O_{2,dis,bio}$ (The full sea ice experiment is intermediate between SI-gasx and SI-bio.) In the circulation experiment, $\Delta C_{dis,bio}$ and $\Delta O_{2,dis,bio}$ are almost orthogonal to the Redfield line, which causes a large deviation from the Redfield estimate of AOU change and deep carbon change. The 'All' experiment, which can be regarded as a sum of the iron fertilization, sea ice and circulation experiments, also falls close to the Redfield line.

ΔAOU also contains a physical disequilibrium component, $\Delta O_{2,dis,phy}$, which can impact its relationship with ΔC_{bio} . In particular, in the sea ice experiment, which shows the largest effect on O₂ of any single parameter examined, both O_{2,dis,bio} and O_{2,dis,phy} are enhanced (become more negative), which leads to a large decrease in the deep ocean oxygen, despite a reduced consumption. However, sea ice has a much smaller effect on glacial carbon storage because physical air-sea disequilibrium serves to decrease DIC, whereas biologically mediated disequilibrium serves to increase DIC by preventing outgassing of carbon-rich upwelled waters, such that there is a cancellation of much of the effect of sea ice on the CO₂ air-sea gas exchange¹⁰. This breaks down the relationship between AOU and biological carbon storage, such that AOU overestimates the change in biological carbon storage by over a factor of three ($\Delta C_{bio} = 99 \text{ PgC}$ and ΔC_{bio} (AOU) = 334 PgC) in this experiment. A similar overestimation was found in the circulation experiment ($\Delta C_{bio} = -102 \, \text{PgC}$ and ΔC_{bio} (AOU) = -253 PgC).

Interestingly, in the 'All' experiment ΔAOU appears to be a good proxy for ΔC_{bio} . However, we note that this is because the change in $C_{\text{dis,phy}}$ is quite small due to the compensating effects from circulation, temperature and sea ice¹0. We believe that, although the effect of different processes on individual oxygen and carbon components in our model is qualitatively quite robust, quantitative changes in those components and their interactions are likely to be model and state dependent (see the 'reverse' experiments in Supplementary Fig. 26). Such a cancellation, and hence the ability of AOU to quantify changes in C_{bio} is therefore unlikely to be robust.

To summarize, the simulated deep ocean deoxygenation in the LGM is consistent with proxy data. Oxygen concentrations decrease despite a reduction in the modelled export production in the glacial ocean, which leads to a reduction in respired carbon (and thus O_2 consumption), that is, a less-efficient biological carbon pump, as conventionally defined. Previous studies^{5,9} instead interpreted the same proxy-based evidence of glacial deoxygenation as implying an increase in the efficiency of the soft-tissue pump. We found, however, that the greater air–sea O_2 disequilibrium during the LGM, caused by an expansion in sea ice cover in the Southern Ocean, along with the increased iron fertilization, provides a better explanation for lower oxygen concentrations in the glacial deep ocean.

Our results also suggest that the observed increase in AOU in the LGM was primarily caused by biologically mediated disequilibrium, compounded by physical disequilibrium. The latter can decouple AOU from biological carbon storage, which implies that caution must be exercised in interpreting quantitative oxygen proxies in terms of carbon storage.

Our model probably does not capture the complex nature of gas exchange in regions such as the Southern Ocean, where it may be

altered by, for example, the presence of leads in sea ice and seasonal polynyas 19,26,40 . To refine our understanding of glacial–interglacial changes in ocean carbon and oxygen distributions, more extensive seasonal observations of O_2 gas exchange, especially in the Southern Ocean, are required. The magnitude of disequilibrium should also be investigated, both in models that do not base respired carbon estimates on AOU and those that incorporate recent developments in using flexible stoichiometry 45,46 . The results of recent studies with such models suggest that this may enhance glacial C_{bio} storage 46,47 and may slightly reduce the quota of O_2 required to respire C_{soft} (ref. 46), which could alleviate deoxygenation.

Online content

Any methods, additional references, Nature Research reporting summaries, source data, extended data, supplementary information, acknowledgements, peer review information; details of author contributions and competing interests; and statements of data and code availability are available at https://doi.org/10.1038/s41561-020-00667-7.

Received: 26 April 2020; Accepted: 10 November 2020; Published online: 4 January 2021

References

- Broecker, W. S. Glacial to interglacial changes in ocean chemistry. Prog. Oceanogr. 11, 151–197 (1982).
- Sigman, D. M., Hain, M. P. & Haug, G. H. The polar ocean and glacial cycles in atmospheric CO₂ concentration. *Nature* 466, 47–55 (2010).
- Jaccard, S. L. & Galbraith, E. D. Large climate-driven changes of oceanic oxygen concentrations during the last deglaciation. *Nat. Geosci.* 5, 151–156 (2012).
- Jacobel, A. W. et al. Deep Pacific storage of respired carbon during the last ice age: perspectives from bottom water oxygen reconstructions. Quat. Sci. Rev. 230, 106065 (2020).
- Bradtmiller, L., Anderson, R., Sachs, J. & Fleisher, M. A deeper respired carbon pool in the glacial equatorial Pacific Ocean. *Earth Planet. Sci. Lett.* 299, 417–425 (2010).
- Galbraith, E. D. & Jaccard, S. L. Deglacial weakening of the oceanic soft tissue pump: global constraints from sedimentary nitrogen isotopes and oxygenation proxies. *Quat. Sci. Rev.* 109, 38–48 (2015).
- Jaccard, S. L., Galbraith, E. D., Martínez-García, A. & Anderson, R. F. Covariation of deep Southern Ocean oxygenation and atmospheric CO₂ through the last ice age. *Nature* 530, 207–210 (2016).
- Anderson, R. F. et al. Deep-sea oxygen depletion and ocean carbon sequestration during the last ice age. Glob. Biogeochem. Cycles 33, 301–317 (2019).
- Yamamoto, A., Abe-Ouchi, A., Ohgaito, R., Ito, A. & Oka, A. Glacial CO₂ decrease and deep-water deoxygenation by iron fertilization from glaciogenic dust. Climate 15, 981–996 (2019).
- Khatiwala, S., Schmittner, A. & Muglia, J. Air–sea disequilibrium enhances ocean carbon storage during glacial periods. Sci. Adv. 5, eaaw4981 (2019).
- Sarmiento, J. L. & Gruber, N. Ocean Biogeochemical Dynamics (Princeton Univ. Press. 2006).
- Stephens, B. B. & Keeling, R. F. The influence of Antarctic sea ice on glacial-interglacial CO₂ variations. *Nature* 404, 171–174 (2000).
- İto, T. & Follows, M. J. Air-sea disequilibrium of carbon dioxide enhances the biological carbon sequestration in the Southern Ocean. *Glob. Biogeochemical Cycles* 27, 1129–1138 (2013).
- 14. Ito, T., Follows, M. J. & Boyle, E. A. Is AOU a good measure of respiration in the oceans? *Geophys. Res. Lett.* **31**, L17305 (2004).
- Wolf, M. K., Hamme, R. C., Gilbert, D., Yashayaev, I. & Thierry, V. Oxygen saturation surrounding deep water formation events in the Labrador Sea from Argo-O₂ data. *Glob. Biogeochem. Cycles* 32, 635–653 (2018).
- Russell, J. L. & Dickson, A. G. Variability in oxygen and nutrients in South Pacific Antarctic Intermediate Water. Glob. Biogeochem. Cycles 17, 1033 (2003).
- Khatiwala, S., Primeau, F. & Holzer, M. Ventilation of the deep ocean constrained with tracer observations and implications for radiocarbon estimates of ideal mean age. *Earth Planet. Sci. Lett.* 325–326, 116–125 (2012).
- Duteil, O. et al. A novel estimate of ocean oxygen utilisation points to a reduced rate of respiration in the ocean interior. *Biogeosciences* 10, 7723–7738 (2013).
- Eggleston, S. & Galbraith, E. D. The devil's in the disequilibrium: multi-component analysis of dissolved carbon and oxygen changes under a broad range of forcings in a general circulation model. *Biogeosciences* 15, 3761–3777 (2018).

- Weaver, A. J. et al. The UVic Earth System Climate Model: model description, climatology, and applications to past, present and future climates. *Atmos. Ocean* 39, 361–428 (2001).
- Schmittner, A. & Somes, C. J. Complementary constraints from carbon (¹³C) and nitrogen (¹⁵N) isotopes on the glacial ocean's soft-tissue biological pump. *Paleoceanography* 31, 669–693 (2016).
- Muglia, J., Skinner, L. C. & Schmittner, A. Weak overturning circulation and high Southern Ocean nutrient utilization maximized glacial ocean carbon. *Earth Planet. Sci. Lett.* 496, 47–56 (2018).
- Schmidtko, S., Stramma, L. & Visbeck, M. Decline in global oceanic oxygen content during the past five decades. *Nature* 542, 335–339 (2017).
- Bopp, L. et al. Multiple stressors of ocean ecosystems in the 21st century: projections with CMIP5 models. *Biogeosciences* 10, 6225–6245 (2013).
- Gottschalk, J. et al. Biological and physical controls in the Southern Ocean on past millennial-scale atmospheric CO₂ changes. Nat. Commun. 7, 11539 (2016).
- 26. Lu, Z. et al. Oxygen depletion recorded in upper waters of the glacial Southern Ocean. *Nat. Commun.* **48**, 829–834 (2016).
- Hoogakker, B. A. A., Elderfield, H., Schmiedl, G., McCave, I. N. & Rickaby, R. E. M. Glacial-interglacial changes in bottom-water oxygen content on the Portuguese margin. *Nat. Geosci.* 8, 40–43 (2015).
- 28. Bunzel, D. et al. A multi-proxy analysis of late quaternary ocean and climate variability for the Maldives, Inner Sea. *Climate* 13, 1791–1813 (2017).
- Hoogakker, B. A. A. et al. Glacial expansion of oxygen-depleted seawater in the eastern tropical Pacific. *Nature* 562, 410–413 (2018).
- Umling, N. E. & Thunell, R. C. Mid-depth respired carbon storage and oxygenation of the eastern equatorial Pacific over the last 25,000 years. *Quat. Sci. Rev.* 189, 43–56 (2018).
- 31. Durand, A. et al. Reduced oxygenation at intermediate depths of the southwest Pacific during the Last Glacial Maximum. *Earth Planet. Sci. Lett.* **491**, 48–57 (2018).
- Lu, W. et al. I/Ca in epifaunal benthic foraminifera: a semi-quantitative proxy for bottom water oxygen in a multi-proxy compilation for glacial ocean deoxygenation. *Earth Planet. Sci. Lett.* 533, 116055 (2020).
- Kohfeld, K. E., Quéré, C. L., Harrison, S. P. & Anderson, R. F. Role of marine biology in glacial-interglacial CO₂ cycles. Science 308, 74–78 (2005).
- Waelbroeck, C. et al. Constraints on the magnitude and patterns of ocean cooling at the Last Glacial Maximum. Nat. Geosci. 2, 127–132 (2009).
- Benz, V., Esper, O., Gersonde, R., Lamy, F. & Tiedemann, R. Last Glacial Maximum sea surface temperature and sea-ice extent in the pacific sector of the southern ocean. Quat. Sci. Rev. 146, 216–237 (2016).
- 36. Matsumoto, K., Hashioka, T. & Yamanaka, Y. Effect of temperature-dependent organic carbon decay on atmospheric $p_{\rm CO2}$. *J. Geophys. Res. Biogeosci.* 112, G02007 (2007).
- Oka, A., Abe-Ouchi, A., Chikamoto, M. O. & Ide, T. Mechanisms controlling export production at the LGM: effects of changes in oceanic physical fields and atmospheric dust deposition. *Glob. Biogeochem. Cycles* 25, GB2009 (2011).

- 38. Schmittner, A., Galbraith, E. D., Hostetler, S. W., Pedersen, T. F. & Zhang, R. Large fluctuations of dissolved oxygen in the Indian and Pacific Oceans during Dansgaard–Oeschger oscillations caused by variations of North Atlantic Deep Water subduction. *Paleoceanography* 22, PA3207 (2007).
- Roche, D. M., Crosta, X. & Renssen, H. Evaluating Southern Ocean sea-ice for the Last Glacial Maximum and pre-industrial climates: PMIP-2 models and data evidence. *Quat. Sci. Rev.* 56, 99–106 (2012).
- Smith, J. A., Hillenbrand, C.-D., Pudsey, C. J., Allen, C. S. & Graham, A. G. C. The presence of polynyas in the Weddell Sea during the last glacial period with implications for the reconstruction of sea-ice limits and ice sheet history. *Earth Planet. Sci. Lett.* 296, 287–298 (2010).
- Zanowski, H., Hallberg, R. & Sarmiento, J. L. Abyssal ocean warming and salinification after Weddell polynyas in the GFDL CM2G coupled climate model. J. Phys. Oceanogr. 45, 2755–2772 (2015).
- Conway, T., Wolff, E., Röthlisberger, R., Mulvaney, R. & Elderfield, H. Constraints on soluble aerosol iron flux to the Southern Ocean at the Last Glacial Maximum. *Nat. Commun.* 6, 7850 (2015).
- Shoenfelt, E. M., Winckler, G., Lamy, F., Anderson, R. F. & Bostick, B. C. Highly bioavailable dust-borne iron delivered to the Southern Ocean during glacial periods. *Proc. Natl Acad. Sci. USA* 115, 11180–11185 (2018).
- 44. Galbraith, E. D. & Skinner, L. C. The biological pump during the Last Glacial Maximum. *Annu. Rev. Mar. Sci.* 12, 559–586 (2020).
- Galbraith, E. D. & Martiny, A. C. A simple nutrient-dependence mechanism for predicting the stoichiometry of marine ecosystems. *Proc. Natl Acad. Sci.* USA 112, 8199–8204 (2015).
- Matsumoto, K., Rickaby, R. & Tanioka, T. Carbon export buffering and CO2 drawdown by flexible phytoplankton C:N:P under glacial conditions. *Paleoceanogr. Paleoclimatol.* 35, e2019PA003823 (2020).
- Ödalen, M. et al. Variable C/P composition of organic production and its effect on ocean carbon storage in glacial-like model simulations. Biogeosciences 17, 2219–2244 (2020).
- 48. Garcia, H. E. et al. World Ocean Atlas 2018 Volume 3: Dissolved Oxygen, Apparent Oxygen Utilization, and Oxygen Saturation (NOAA, 2018).
- Drucker, R. & Riser, S. C. In situ phase-domain calibration of oxygen Optodes on profiling floats. *Methods Oceanogr.* 17, 296–318 (2016).
- Johnson, K. S. et al. SOCCOM Float Data—Snapshot 2017-06-06 (UC San Diego Library Digital Collections, 2017).
- Gottschalk, J. et al. Carbon isotope offsets between benthic foraminifer species of the genus *Cibicides* (*Cibicidoides*) in the glacial sub-Antarctic Atlantic. *Paleoceanography* 31, 1583–1602 (2016).

Publisher's note Springer Nature remains neutral with regard to jurisdictional claims in published maps and institutional affiliations.

 $\mbox{\@0mu}$ The Author(s), under exclusive licence to Springer Nature Limited 2021, corrected publication 2021

Methods

Model description. The model set up used for this study is described in Khatiwala et al.10 and references therein. Briefly, the biogeochemical model used is MOBI (Model of Ocean Biogeochemistry and Isotopes), which has the limiting nutrients dissolved nitrogen, phosphorus and iron, two phytoplankton functional groups, one zooplankton class, dissolved and particulate organic matter and DIC, O, and alkalinity21. All the components of the model track carbon and nitrogen isotopes. The interactive iron cycle is driven externally from atmospheric dust, sediments and hydrothermal vent inputs⁵². Monthly climatologies of atmospheric soluble iron fluxes are used that were generated using monthly dust flux climatologies of both PIC and LGM53, using a constant iron dust content of 3.5% (ref. 54) and a fitted function of iron flux and iron solubility⁵². The dust flux climatologies were constructed by interpolation of Holocene and glacial dust flux data from terrestrial and marine sediments, and ice cores, primarily from the DIRTMAP 3 database⁵ In the Southern Ocean south of 35°S, the LGM soluble iron flux is multiplied by ten, which places the estimate in line with Antarctic ice cores⁴² and marine sediment cores⁴³ and results in a substantially better fit²² between the simulated and observed $\delta^{15}N$ and glacial–interglacial export production changes (Supplementary Fig. 3). The sedimentary release of dissolved iron is proportional to the flux of organic carbon at the ocean bottom⁵²; for the LGM the subgrid bathymetry used to calculate this was adjusted for the 110 m glacial sea level drop55. MOBI is coupled to the Transport Matrix Method (TMM)⁵⁶⁻⁵⁸, a framework for computationally efficient offline tracer simulations

MOBI-TMM is driven by surface winds, circulation, temperature, salinity and sea ice from UVic ESCM (version 2.9)20, a three-dimensional ocean general circulation model (1.8° × 3.6° × 19 layers) coupled to a one-layer atmospheric energy-moisture balance, dynamic-thermodynamic sea ice and land surface models. The PIC and LGM simulations used were tuned to a suite of modern biogeochemical and LGM sedimentary isotope records (δ^{13} C, Δ^{14} C and δ^{15} N), as previously described^{22,59}. Briefly, the LGM simulation was forced with atmospheric CO₂ and orbital parameters in accord with 19 kyr BP, the addition of a multimodel mean LGM anomaly wind field stress from PMIP3 (Paleoclimate Intercomparison Project Phase 3) to the present day climatological field, a PMIP3 reconstruction of the continental ice sheet⁶⁰ and a global addition of 1 PSU to salinity consistent with a glacial sea level drop. The consistency of the simulated large-scale tracer distributions with observations has been demonstrated previously for the equilibrium solutions^{10,22}. The characteristics of the model's LGM state are consistent with observational studies, namely, colder global mean temperature $(\Delta T = -2.5 \,^{\circ}\text{C} \text{ compared to } -2.6 \,^{\circ}\text{C} \text{ from ice-core noble gas measurements}^{61})$ and patterns of sea surface temperature change^{34,35}, a weaker (by ~50%) and shallower Atlantic Meridional Circulation (as implied by the δ^{13} C distribution and ~600-year-older Δ^{14} C deep ocean ages 62,63), 50% more sea ice than in the PIC such that the Southern Ocean maximum (winter) cover was 3×10^{13} m², slightly less than reconstructions (4×10¹³ m²) (ref. ³⁹), and enhanced surface iron fluxes to the Southern Ocean (required to reproduce observed δ^{13} C (ref. ²²) and δ^{15} N data).

Oxygen decomposition. To track O_2 through the model, total O_2 is expressed as the sum of $O_{2,pre}$ and $O_{2,soft}$ (equation (3)):

$$O_2 = O_{2,pre} + O_{2,soft} \tag{3}$$

A preformed tracer is a conservative tracer whose value is set at the surface of the ocean and is passively transported into the interior by the circulation. $O_{2,soft}$ is negative as respiration removes O_2 , whereas respired carbon (C_{soft}) is positive as it is released when soft tissue is regenerated. $O_{2,soft}$ and C_{soft} are calculated as:

$$O_{2,\text{soft}} = (-1/R_{\text{C:-O}_2}) \times C_{\text{soft}}$$
(4)

$$C_{\text{soft}} = R_{\text{C:P}} \times PO_{4,\text{reg}} \tag{5}$$

$$PO_{4,reg} = PO_4 - PO_{4,pre} \tag{6}$$

where we relate $O_{2,soft}$, C_{soft} and regenerated phosphate (PO_{4,reg}) via a fixed Redfield stoichiometry for C:P: $-O_2$. The phosphate inventory is fixed in the ocean model, and to calculate PO_{4,reg}, we simulated a preformed phosphate (PO_{4,pre}) tracer for each experiment by propagating the seasonally varying surface ocean phosphate field into the interior using the TMM. The difference between PO₄ and PO_{4,pre} at the end of each run is the regenerated phosphate (equation (6)).

To simulate $O_{2,pre}$ we similarly propagated the seasonally varying surface ocean oxygen field into the interior. $O_{2,pre}$ is further decomposed into equilibrium and disequilibrium components by simulating an additional tracer, $O_{2,eq}$, by propagating the surface theoretical equilibrium oxygen into the interior. $O_{2,pre}$ and $O_{2,eq}$ were simulated for each experiment and the disequilibrium component $O_{2,dis}$ of $O_{2,pre}$ is the difference between the two.

The O_2 decomposition in equation (3) is thus more completely described by:

$$O_2 = \underbrace{O_{2,\text{eq}} + O_{2,\text{dis},\text{phy}} + O_{2,\text{dis},\text{bio}}}_{O_{2,\text{pre}}} + \underbrace{(-R_{-O_2:P}) \times PO_{4,\text{reg}}}_{O_{2,\text{soft}}} \tag{7}$$

 $R_{-{\rm O}_2;{\rm P}}$ is the constant oxygen-to-phosphate Redfield stoichiometry. For every experiment, we also ran a parallel simulation in which the physical forcings (circulation, temperature, salinity, winds and so on) were the same, but the source/ sink terms in the biogeochemical model were switched off. Nutrients, DIC and O_2 were all transported by the TMM, but did not get used in biological processes. As such, this parallel simulation gave us a reference point for the ocean without any biological activity. $O_{2,eq}$ which only depends on temperature and salinity, is identical in the full physical–biogeochemical simulation and physics-only simulation. The disequilibrium component of $O_{2,pre,phy}$ is then purely a result of physical processes (for example, temperature gradients and sea ice blocking gas exchange) for the conditions of that simulation (equation (8)). In the parallel full physical–biogeochemical simulations, biological processes change the distribution of DIC and O_2 , and thus change the O_2 disequilibrium. We attribute any difference in disequilibrium between the full and physics-only experiments to biological processes (equation (9)):

$$O_{2,dis,phy} = O_{2,pre,phy} - O_{2,eq}$$

$$\tag{8}$$

$$O_{2,dis,bio} = O_{2,dis} - O_{2,dis,phy}$$

$$(9)$$

Equilibrium and perturbation experiments. All equilibrium and perturbation tracer simulations were run for 10,000 years to steady state. The procedure of running parallel sets of physics-only and full simulations was carried out for the PIC and LGM equilibrium experiments, as well as for all perturbation experiments. In the physics-only simulations for the perturbation experiments, the model was started from the steady state of the corresponding physics-only base run (for example, PIC for PIC → LGM perturbations), whereas for the full physical-biogeochemical perturbation simulations the model was started from the steady state of the corresponding full base run. The perturbations applied were the same in both cases. At the end of each perturbation run, the decomposition was performed, as explained above, and differences from the respective base states gave us the perturbation effect on each oxygen component. The 'All' perturbation experiment, in which temperature, circulation, sea ice, iron fertilization and salinity (to account for the 110 m drop in LGM sea level) were simultaneously perturbed, did not exactly reproduce the LGM equilibrium simulation as it still uses the PIC conditions for light, freshwater fluxes and subgrid bathymetry, which affects the sedimentary release of organic carbon.

Decomposition of AOU into oxygen components. We expressed AOU in terms of its components:

$$\begin{aligned} \text{AOU} &= O_{2,\text{sat}} - O_2 \\ &= O_{2,\text{sat}} - \left[O_{2,\text{eq}} + O_{2,\text{soft}} + O_{2,\text{dis,bio}} + O_{2,\text{dis,phy}} \right] \\ &\approx O_{2,\text{sat}} - \left[O_{2,\text{sat}} + O_{2,\text{soft}} + O_{2,\text{dis,bio}} + O_{2,\text{dis,phy}} \right] \\ &= - \left[O_{2,\text{soft}} + O_{2,\text{dis,bio}} + O_{2,\text{dis,phy}} \right] \end{aligned}$$

where we approximated $O_{2,eq}$ by $O_{2,sat}$. Thus, a change in AOU can be written as:

$$\Delta AOU \approx -\Delta O_{2,soft} - \Delta O_{2,dis,bio} - \Delta O_{2,dis,phy}$$

Data availability

The model output that support the findings of this study are available from https://doi.org/10.5281/zenodo.4078981. World Ocean Atlas data were obtained from https://www.nodc.noaa.gov/OC5/woa18/, and float data from the SOCCOM website https://soccom.princeton.edu/.

Code availability

Model codes are available from https://github.com/samarkhatiwala/tmm.

References

- Muglia, J., Somes, C. J., Nickelsen, L. & Schmittner, A. Combined effects of atmospheric and seafloor iron fluxes to the glacial ocean. *Paleoceanography* 32, 1204–1218 (2017).
- Lambert, F. et al. Dust fluxes and iron fertilization in Holocene and Last Glacial Maximum climates. Geophys. Res. Lett. 42, 6014–6023 (2015).
- Mahowald, N. M. et al. Atmospheric iron deposition: global distribution, variability, and human perturbations. Annu. Rev. Mar. Sci. 1, 245–278 (2008).
- Lambeck, K., Rouby, H., Purcell, A., Sun, Y. & Sambridge, M. Sea level and global ice volumes from the Last Glacial Maximum to the Holocene. *Proc. Natl Acad. Sci. USA* 111, 15296–15303 (2014).
- Khatiwala, S., Visbeck, M. & Cane, M. A. Accelerated simulation of passive tracers in ocean circulation models. Ocean Model. 9, 51–69 (2005).
- Khatiwala, S. A computational framework for simulation of biogeochemical tracers in the ocean. Glob. Biogeochem. Cycles 21, GB3001 (2007).
- Khatiwala, S. Transport Matrix Method Software for Ocean Biogeochemical Simulations https://doi.org/10.5281/Zenodo.1246300 (2018).

- Muglia, J. & Schmittner, A. Glacial Atlantic overturning increased by wind stress in climate models. *Geophys. Res. Lett.* 42, 9862–9868 (2015).
- Abe-Ouchi, A. et al. Ice-sheet configuration in the CMIP5/PMIP3 Last Glacial Maximum experiments. Geosci. Model Dev. 8, 3621–3637 (2015).
- Bereiter, B., Shackleton, S., Baggenstos, D., Kawamura, K. & Severinghaus, J. Mean global ocean temperatures during the last glacial transition. *Nature* 553, 39–44 (2018).
- Sarnthein, M., Schneider, B. & Grootes, P. M. Peak glacial ¹⁴C ventilation ages suggest major draw-down of carbon into the abyssal ocean. *Climate* 9, 2595–2614 (2013).
- Skinner, L. C. et al. Radiocarbon constraints on the glacial ocean circulation and its impact on atmospheric CO₂. Nat. Commun. 8, 16010 (2017).

Acknowledgements

This study was supported by UK NERC grants NE/M020835/1 and NE/T009357/1 to S.K., and US National Science Foundation grant OCE-1924215 to A.S. E.C. acknowledges support from the Rhodes Trust. Computing resources were provided by the Climate Simulation Laboratory at NCAR's Computational and Information Systems Laboratory (ark:/85065/d7wd3xhc), sponsored by the National Science Foundation and other agencies, and the University of Oxford Advanced Research Computing (ARC) facility (https://doi.org/10.5281/zenodo.22558). Data shown in Fig. 1 were collected and

made freely available by the Southern Ocean Carbon and Climate Observations and Modeling (SOCCOM) Project funded by the National Science Foundation, Division of Polar Programs (NSF PLR -1425989), supplemented by NASA, and by the International Argo Program and the NOAA programmes that contribute to it. The Argo Program is part of the Global Ocean Observing System.

Author contributions

S.K. and A.S. designed the study; S.K. carried out the experiments; all the authors analysed the results; E.C. wrote the manuscript with input from S.K. and A.S.

Competing interests

The authors declare no competing interests.

Additional information

Supplementary information is available for this paper at https://doi.org/10.1038/s41561-020-00667-z.

Correspondence and requests for materials should be addressed to E.C.

Reprints and permissions information is available at www.nature.com/reprints.